ESI for

Controllable 1D, 2D and 3D supramolecular assemblies of Ir(III) complexes

Yifan Lin,[a] Yan Chen,[a] Rui Cai,[a] Hao Zhang*[b] and Chun Liu*[a]

[a] State Key Laboratory of Fine Chemicals, Frontier Science Center for Smart Materials, School of Chemical Engineering, Dalian University of Technology, Dalian 116024, China. E-mail: cliu@dlut.edu.cn

[b] School of Chemistry and Chemical Engineering, State Key Laboratory Incubation Base for Green Processing of Chemical Engineering, Shihezi University, Shihezi 832003, Xinjiang, China. E-mail: haozhang@shzu.edu.cn

Contents

Materials and methods

Materials and instruments

All starting materials were purchased from commercial suppliers and used without further purification. The solvents were treated as required prior to use. NMR spectra were recorded on a 400 MHz Bruker Avance II 400 or a 500 MHz Bruker AVANCE III 500. Mass spectra were recorded with a Synapt G2-Si HDMS mass spectrometer. UV-Vis absorption spectra were recorded with an Agilent Cary 100 UV-Vis spectrophotometer equipped with magnetic stirring and temperature control. Emission spectra were recorded with a HITACHI F-7100 fluorescence spectrophotometer. Scanning electron microscope (SEM) images were obtained on JSM-7610F Plus. The dynamic light scattering (DLS) were performed on Malvern ZS90. Atomic force microscope (AFM) images were obtained on JPK Nanowizard 4XP. The powder XRD (PXRD) diffractograms were obtained on Bruker D8 Advance X-ray diffractometer. The measurement was performed from 5 ° to 50 ° and the scanning speed was 5 degrees per minute.

Synthetic routes of cyclometalating ligands and Ir(III) complexes 1-3

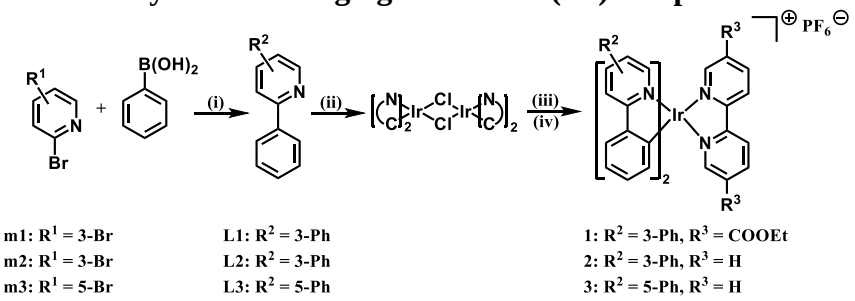

Figure S1. Synthetic routes of **1**, **2** and **3**. (i) $Pd(OAc)_2$, K_2CO_3, Air, $EtOH/H_2O$, 3:1(v/v), 80 ℃, 10-30 min. (ii) $IrCl_3$ $3H_2O$, $EtOCH_2CH_2OH/H_2O$, 3:1 (v/v), 120 ℃, N_2, 24 h. (iii) **1**: diethyl 2,2'-bipyridine-5,5'-dicarboxylate, $EtOCH_2CH_2OH$ 8 mL, 120 ℃, N_2, 24 h. **2**, **3**: 2,2'-bipyridine, $EtOCH_2CH_2OH$ 8 mL, 120 ℃, N_2, 24 h. (iv) KPF_6, RT, 24 h.

Synthetic steps of ligands L1, L2 and L3

A mixture of 2-bromopyridine derivatives (1 mmol), 3 equiv. of phenylboronic acid, 2 equiv. of K_2CO_3, $Pd(OAc)_2$ (1.5 mol%), $EtOH/H_2O$ (3:1 v/v) was stirred at 80 ℃ in air for the indicated time. The reaction mixture was added to brine (15 mL) and extracted with dichloromethane. The solvent was concentrated under vacuum, and the product was isolated by column chromatography.

Synthetic steps of Ir(III) complexes 1-3

The $IrCl_3$ $3H_2O$ (0.2 mmol) was reacted with 2.5 equiv. of the cyclometalating ligand in a mixture of 2-ethoxyethanol and water (6 mL/2 mL) at 120 ℃ under nitrogen for 24 h. Upon cooling to room temperature, the suspension was concentrated under vacuum. The solid was completely dried to give the crude cyclometalated Ir(III) chloride-bridged dimer. Without further purification, the dimeric Ir(III) complex was subsequently reacted with 3 equiv. of the diethyl 2,2'-bipyridine-5,5'-dicarboxylate or 2,2'-bipyridine in 2-ethoxyethanol at 120 ℃ under nitrogen for 24 h. After cooling to room temperature, a 10-fold excess of KPF_6 saturated aqueous solution was added and stirred for 24 h. The reaction mixture was added to brine (15 mL) and extracted with dichloromethane. The product was isolated by column chromatography.

Characterization of Ir(III) complexes 1-3

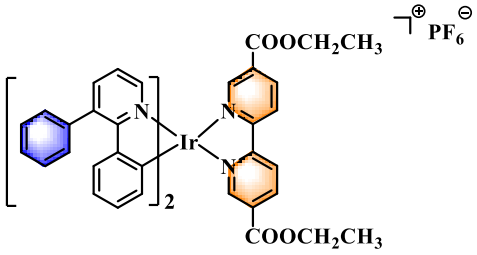

1: a brown solid, yield 82%; ^{1}H NMR (400 MHz, DMSO-d_6) δ 9.14 (d, J = 8.3 Hz, 2H), 8.72 (dd, J = 8.4, 2.0 Hz, 2H), 8.39 (d, J = 1.7 Hz, 2H), 7.90 (dd, J = 5.7, 1.4 Hz, 2H), 7.75 (dd, J = 7.7, 1.4 Hz, 2H), 7.57 (d, J = 2.2 Hz, 6H), 7.41 (d, J = 30.7 Hz, 4H), 7.16 (dd, J = 7.7, 5.8 Hz, 2H), 6.94 - 6.84 (m, 2H), 6.75 - 6.50 (m, 4H), 6.38 (d, J = 7.4 Hz, 2H), 4.36 - 4.21 (m, 4H), 1.20 (q, J = 6.8 Hz, 6H); ^{13}C NMR (125 MHz, DMSO-d_6) δ 163.67, 162.53, 162.44, 157.38, 157.25, 151.08, 151.01, 150.35, 149.28, 144.09, 144.06, 141.47, 140.01, 139.86, 138.79, 136.51, 131.27, 131.18, 130.04, 129.91, 129.58, 129.29, 128.64, 126.17, 126.08, 123.22, 121.33, 67.21, 65.58, 65.30, 61.86, 30.87, 21.98, 14.98, 13.87, 13.65. HRMS (Synapt G2-Si HDMS, *m/z*): calcd for $C_{50}H_{40}N_4O_4Ir$ $[M - PF_6]^+$ 953.2679, found 953.2679. HRMS (LTQ Orbitrap XL, *m/z*): calcd for PF_6^- 144.9642, found 144.9654.

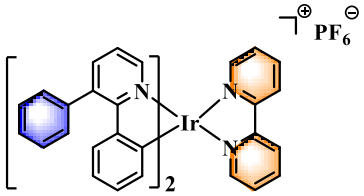

2: a yellow solid, yield 68%; ^{1}H NMR (400 MHz, DMSO-d_6) δ 8.93 (d, J = 8.2 Hz, 2H), 8.31 (t, J = 7.8 Hz, 2H), 7.86 (d, J = 5.1 Hz, 2H), 7.80 - 7.67 (m, 6H), 7.63 - 7.42 (m, 8H), 7.31 (s, 2H), 7.23 - 7.13 (m, 2H), 6.82 (t, J = 7.2 Hz, 2H), 6.66 - 6.52 (m, 4H), 6.30 (d, J = 7.5 Hz, 2H); ^{13}C NMR (125 MHz, DMSO-d_6) δ 163.98, 155.27, 152.27, 149.64, 148.52, 144.12, 141.34, 139.77, 138.91, 136.58, 131.07, 129.55, 129.18, 128.61, 125.19, 123.21, 121.15. HRMS (Synapt G2-Si HDMS, *m/z*): calcd for $C_{44}H_{32}N_4Ir$ $[M - PF_6]^+$ 809.2251, found 809.2251.

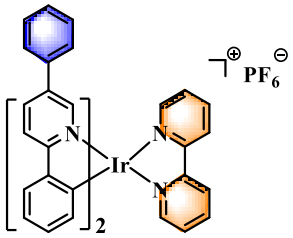

3: a yellow solid, yield 90%; ^{1}H NMR (400 MHz, DMSO-d_6) δ 8.88 (d, J = 8.2 Hz, 2H), 8.39 (d, J = 8.6 Hz, 2H), 8.31 (dd, J = 12.6, 6.3 Hz, 4H), 8.04 (d, J = 5.3 Hz, 2H), 8.00 (d, J = 7.7 Hz, 2H), 7.80 - 7.72 (m, 2H), 7.64 (s, 2H), 7.41 (t, J = 6.3 Hz, 6H), 7.37 (d, J = 7.8 Hz, 4H), 7.06 (t, J = 7.5 Hz, 2H), 6.95 (t, J = 7.4 Hz, 2H), 6.31 (d, J = 7.5 Hz, 2H); ^{13}C NMR (125 MHz, DMSO-d_6) δ 165.92, 155.70, 150.42, 150.04, 145.36, 143.37, 139.71, 136.88, 135.18, 134.75, 131.02, 130.50, 129.35, 128.88, 128.77, 126.28, 125.36, 122.44, 120.28; HRMS (Synapt G2-Si HDMS, m/z): calcd for $C_{44}H_{32}N_4Ir$ $[M - PF_6]^+$ 809.2251, found 809.2251.

Sample preparation

SEM and AFM samples were prepared by volatilization of suspensions on the substrates. Nanoparticle (**NP**) samples were prepared immediately after fresh preparation of the corresponding suspensions, and nanofiber (**NF**), nanosheet (**NS**) and nanoblock (**NB**) samples were prepared after waiting for the corresponding equilibrium time. The samples used for the PXRD diffraction patterns were obtained by allowing complexs **1**-**3** to stand with the corresponding H_2O/EtOH or H_2O/CH_3CN conditions (**1**: 75:25, **2**: 85:15, **3**: 90:10, v/v) until the self-assembly equilibrium was reached, followed by centrifugation and drying.

Single crystals

The single crystals of complexes **1**-**3** were cultivated by solvent diffusion in the CH_3CN/H_2O system. Summary of crystallographic data and details of data collection for complexes **1**-**3** are given in Table S4. Single crystals with suitable dimensions were selected under an optical microscope and mounted onto a glass fiber for data collection. Intensity data for **1**-**3** were collected on a Bruker D8 Quest single-crystal X-ray diffractometer equipped with a Photon-3 CMOS detector and a Mo-Kα (λ = 0.71073 Å) radiation source at 200 K. The data integration and reduction were processed using the SMART and SAINT software.[1, 2] The structures were solved by direct methods using SHELXTL and refined on F^2 by the full-matrix least-squares method using the programs SHELXL-2017 and Olex2.[3, 4] All the non-hydrogen atoms were refined with anisotropic thermal displacement coefficients. Hydrogen atoms were fixed geometrically at calculated positions and allowed to ride on the parent non-hydrogen atoms. The X-ray crystallographic coordinates for structures of **1**-**3** have been deposited at the Cambridge Crystallographic Data Centre (CCDC) under deposition numbers CCDC 2268065, 2268064 and 2268063, respectively. These data can be obtained free of charge from the Cambridge Crystallographic Data Centre via www.ccdc.cam.ac.uk/data_request/cif.

Thermodynamic study

Firstly, taking complex **1** as an example, the suspension of **1NP** in H_2O/EtOH (85:15, v/v) was directly prepared inside a quartz cuvette equipped with a magnetic stirrer (25 μM, 800 rpm). After the conversion of **1NP** to **1NF** was finished, the same concentration EtOH solution of monomer **1** was added until the assemblies completely depolymerized into monomers, and the depolymerization experiment completed. Based on the depolymerization curve, the appropriate water content (H_2O/EtOH, 75:25, v/v, 25 μM) was selected for thermodynamic study.

Cooling process: the above suspension of **1NF** in H_2O/EtOH (75:25, v/v, 25 μM) heated up to 348 K and was left at this temperature for 10 min to fully depolymerize **1NF** into monomers. The absorption spectra were recorded with a cooling step of 1 K and cooling rate of 1 K min^{-1} with 30 seconds of equilibration time.

Nucleation-Elongation model for cooperative supramolecular polymerization

The equilibrium between the monomer and the thermodynamic species can be described in a cooperative process with the Nucleation-Elongation model developed by Ten Eikelder, Markvoort and Meijer.[5,6] The values for ΔH^0, ΔS^0, ΔH^0_{nucl} and T_e used in the Nucleation-Elongation model can be determined by a non-linear least-square analysis of the experimental melting curves of the single-component system. These melting curves were obtained by temperature-dependent UV-vis spectroscopy in this work. The equilibrium constants associated with the nucleation and elongation phases can be calculated using equations (1) and (2).

Nucleation step: $K_{nucl} = e^{\left(\frac{-((\Delta H^0 - \Delta H^0_{nucl}) - T\Delta S^0)}{RT}\right)}$ (1)

Elongation step: $K_{el} = e^{\left(\frac{-(\Delta H^0 - T\Delta S^0)}{RT}\right)}$ (2)

Cooperativity factor: $\sigma = \frac{K_{nucl}}{K_{el}} = e^{\left(\frac{\Delta H^0_{nucl}}{RT}\right)}$ (3)

Gibbs free energy: $\Delta G^0 = \Delta H^0 - T\Delta S^0$ (4)

Where ΔG_0 = standard Gibbsfree energy; ΔH^0_{nucl} = nucleation enthalpy; ΔH^0 = enthalpy difference; ΔS^0 = entropy difference; T_e = elongation temperature; K_{nucl} = equilibrium constant of the nucleation process; K_{el} = equilibrium constant of the elongation process; σ = cooperativity factor (K_{nucl}/K_{el}). Gibbs free energy and all the equilibrium constants were calculated at 298 K.

Time-dependent self-assembly

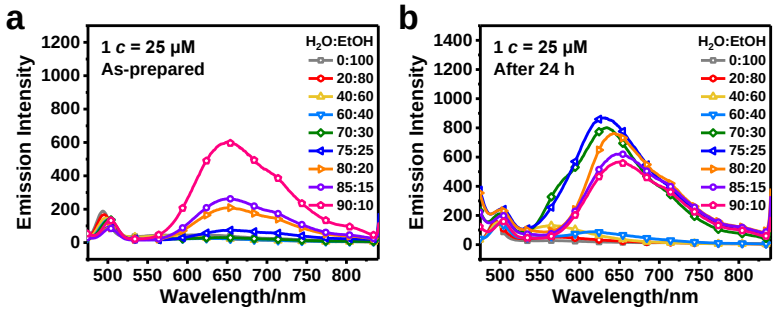

Figure S2. Emission spectra of **1** in H_2O/EtOH (25 μM, freshly prepared (a) and after 24 h (b)) at different ratios. 298 K. λ_{ex} = 430 nm.

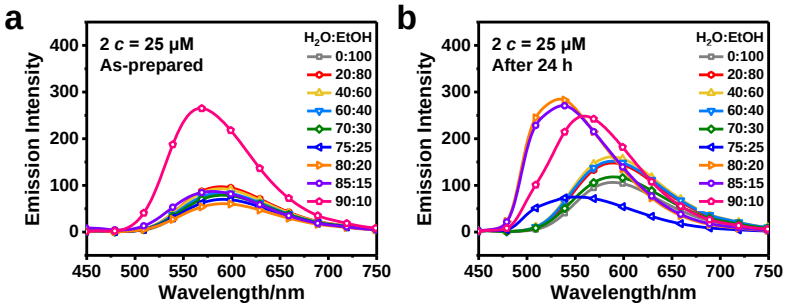

Figure S3. Emission spectra of **2** in H_2O/EtOH (25 μM, freshly prepared (a) and after 24 h (b)) at different ratios. 298 K. λ_{ex} = 400 nm.

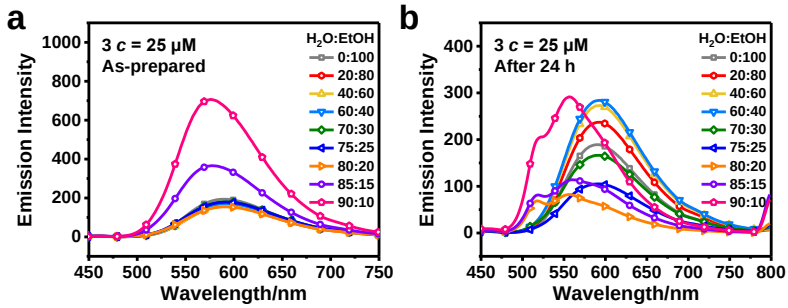

Figure S4. Emission spectra of **3** in H_2O/EtOH (25 μM, freshly prepared (a) and after 24 h (b)) at different ratios. 298 K. λ_{ex} = 400 nm.

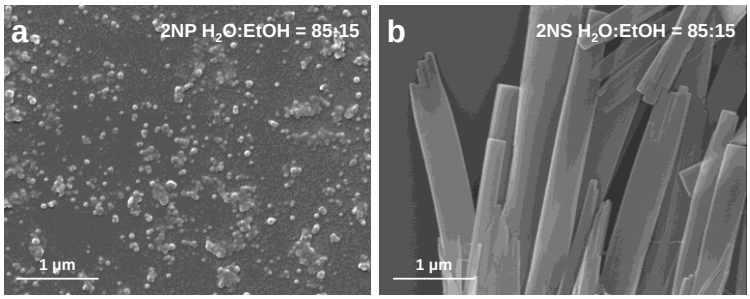

Figure S5. SEM images of **2NP** (a) and **2NS** (b) in H_2O/EtOH (85:15, v/v, 25 μM) at 298 K, respectively.

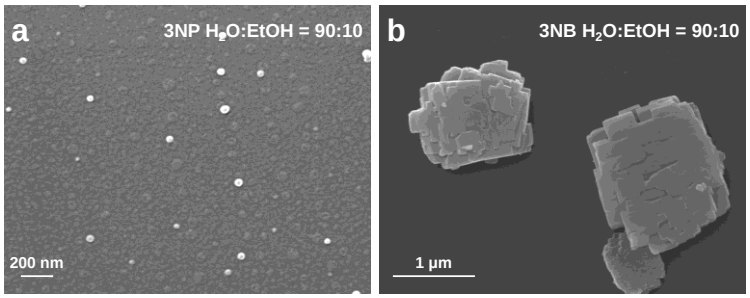

Figure S6. SEM images of **3NP** (a) and **3NB** (b) in H_2O/EtOH (90:10, v/v, 25 μM) at 298 K, respectively.

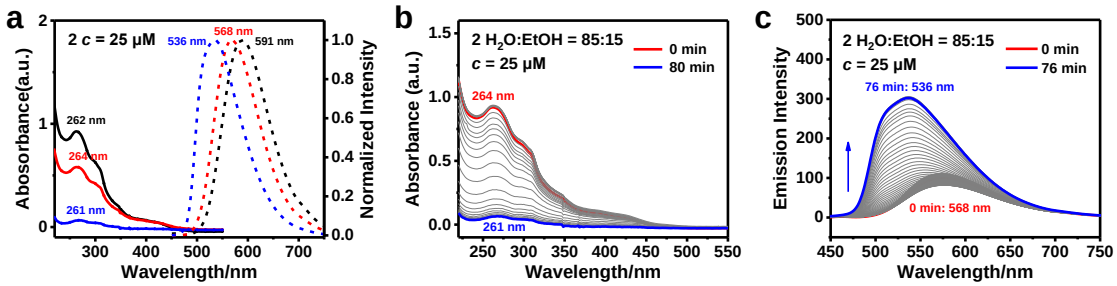

Figure S7. (a) Absorption (solid trace) and emission (dotted trace) spectra of **2** monomer (in EtOH, 25 μM, black line), **2NP** in H_2O/EtOH (85:15, v/v, 25 μM, red line) and **2NS** in H_2O/EtOH (85:15, v/v, 25 μM, blue line). Time-dependent UV-Vis absorption spectra (b) and emission spectra (c) of **2** in H_2O/EtOH (85:15, v/v, 25 μM) at 298 K, λ_{ex} = 400 nm.

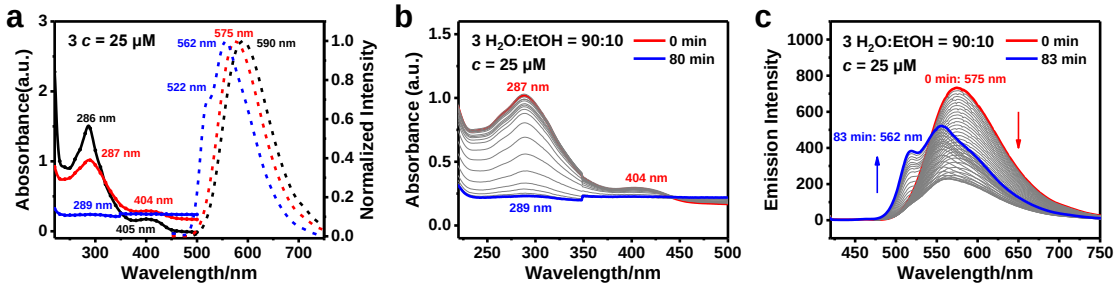

Figure S8. (a) Absorption (solid trace) and emission (dotted trace) spectra of **3** monomer (in EtOH, 25 μM, black line), **3NP** in H_2O/EtOH (90:10, v/v, 25 μM, red line) and **3NB** in H_2O/EtOH (90:10, v/v, 25 μM, blue line). Time-dependent UV-Vis absorption spectra (b) and emission spectra (c) of **3** in H_2O/EtOH (90:10, v/v, 25 μM) at 298 K, λ_{ex} = 400 nm.

Table S1. The characteristic absorption wavelength and the maximum emission wavelength of complexes **1-3**.

Complexes	Species	λ_{abs} (nm)[a]	λ_{em} (nm)[b]
	monomer	**258** (1.20)	**500**
1	**1NP**[c]	**260** (0.94)	503, **651**
	1NF[d]	**265** (0.34)	500, **627**
	monomer	**262** (0.93)	**591**
2	**2NP**[e]	**264** (0.58)	**568**
	2NS[f]	**261** (0.06)	**536**
	monomer	**286** (1.51), 405 (0.17)	**590**
3	**3NP**[g]	**287** (1.02), 404 (0.29)	**575**
	3NB[h]	**290** (0.24)	522, **562**

[a]The absorption maxima are the values in bold style. [b]The emission wavelength maxima are the values in bold style. [c]Suspension of **1NP** in H_2O/EtOH (75:25, v/v, 25 μM). [d]Suspension of **1NF** in H_2O/EtOH (75:25, v/v, 25 μM). [e]Suspension of **2NP** in H_2O/EtOH (85:15, v/v, 25 μM). [f]Suspension of **2NS** in H_2O/EtOH (85:15, v/v, 25 μM). [g]Suspension of **3NP** in H_2O/EtOH (90:10, v/v, 25 μM). [h]Suspension of **3NB** in H_2O/EtOH (90:10, v/v, 25 μM).

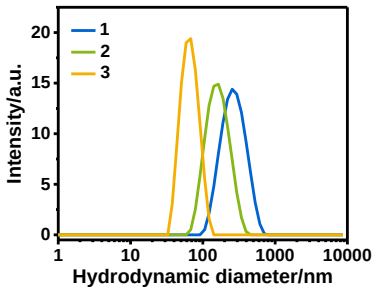

Figure S9. DLS analysis of freshly prepared **1NP** in H_2O/EtOH (75:25, v/v, 25 μM), **2NP** in H_2O/EtOH (85:15, v/v, 25 μM) and **3NP** in H_2O/EtOH (90:10, v/v, 25 μM) respectively.

Table S2. Hydrodynamic diameters and polydispersity index (PDI) of **1NP**, **2NP** and **3NP** in H_2O/EtOH (75:25, 85:15 and 90:10, v/v, 25 μM).

Species-Water contents	Size/nm	PDI
1NP-75%	281	0.141
2NP-85%	169	0.199
3NP-90%	68	0.164

Thermodynamic and kinetic study

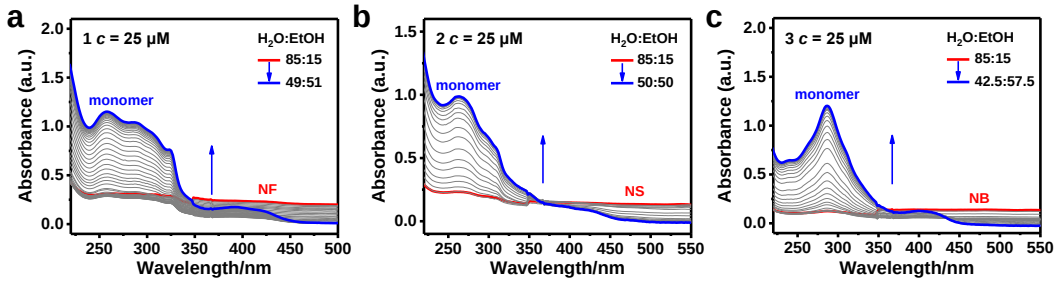

Figure S10. Denaturation UV-Vis studies of **1NF** (a), **2NS** (b) and **3NB** (c) in H_2O/EtOH at 25 μM.

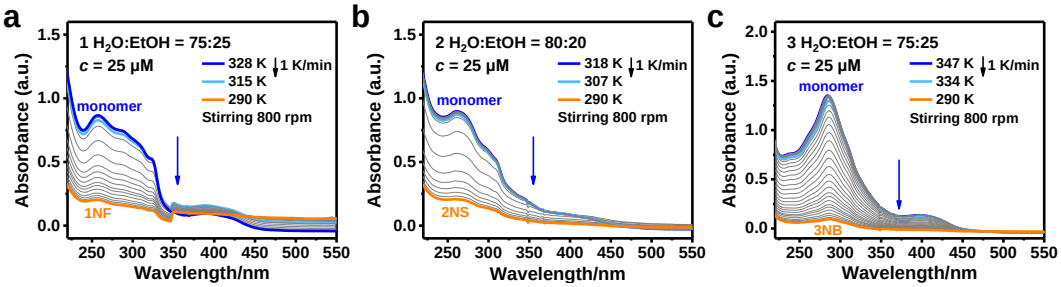

Figure S11. Temperature-dependent UV-Vis absorption spectra of **1NF** in H_2O/EtOH (75:25, v/v) (a), **2NS** in H_2O/EtOH (80:20, v/v) (b) and **3NB** in H_2O/EtOH (75:25, v/v) (c) at 25 μM (cooling rate: 1 K/min).

Table S3. Thermodynamic parameters obtained from temperature-dependent UV-vis experiments of **1**-**3**.

Complex	ΔH^0/ kJ mol^{-1}	ΔS^0/ kJ mol^{-1} K^{-1}	ΔH^0_{nucl}/ kJ mol^{-1}	T_e/K	ΔG^0/ kJ mol^{-1}	K_{nucl}	K_{el}	σ
1	-90.88	-0.20	-23.72	315.03	-31.17	20.24	290708	0.000070
2	-172.34	-0.48	-13.06	306.42	-29.89	893.75	173771	0.005143
3	-45.64	-0.05	-16.21	333.88	-30.50	319.81	222043	0.001440

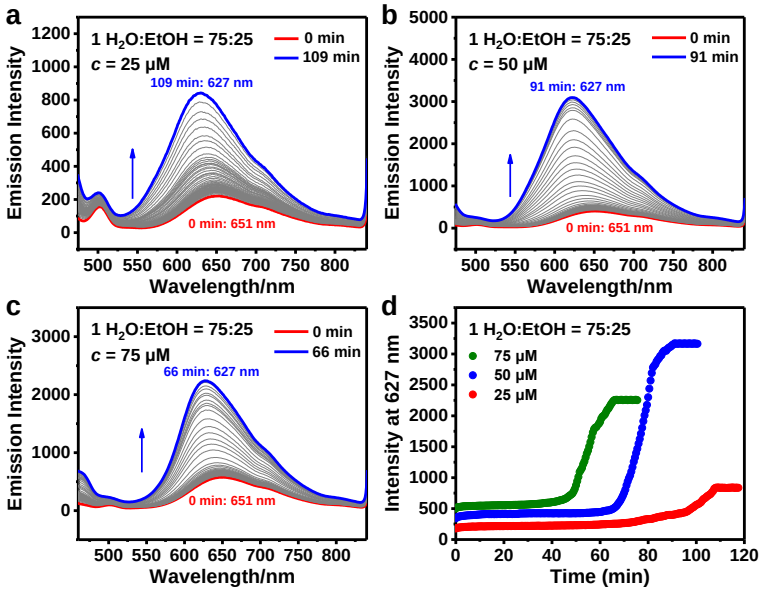

Figure S12. Time-dependent emission spectra of **1** in H_2O/EtOH (75:25, v:v) at different concentrations: 25 μM (a), 50 μM (b), 75 μM (c), respectively, 298 K. (d) Time-dependent emission intensity of **1** (emission intensity at 627 nm) at different initial concentrations in H_2O/EtOH (75:25, v/v), 298 K. λ_{ex} = 430 nm.

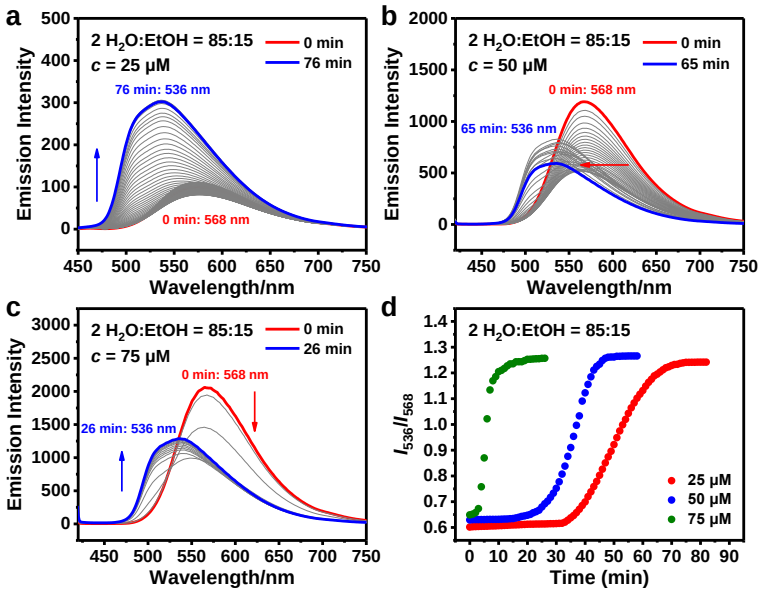

Figure S13. Time-dependent emission spectra of **2** in H_2O/EtOH (85:15, v:v) at different concentrations: 25 μM (a), 50 μM (b), 75 μM (c), respectively, 298 K. (d) Time-dependent relative emission intensity ratios of **2** (emission intensity at 536 nm/568 nm, I_{536}/I_{568}) at different initial concentrations in H_2O/EtOH (85:15, v/v), 298 K. λ_{ex} = 400 nm.

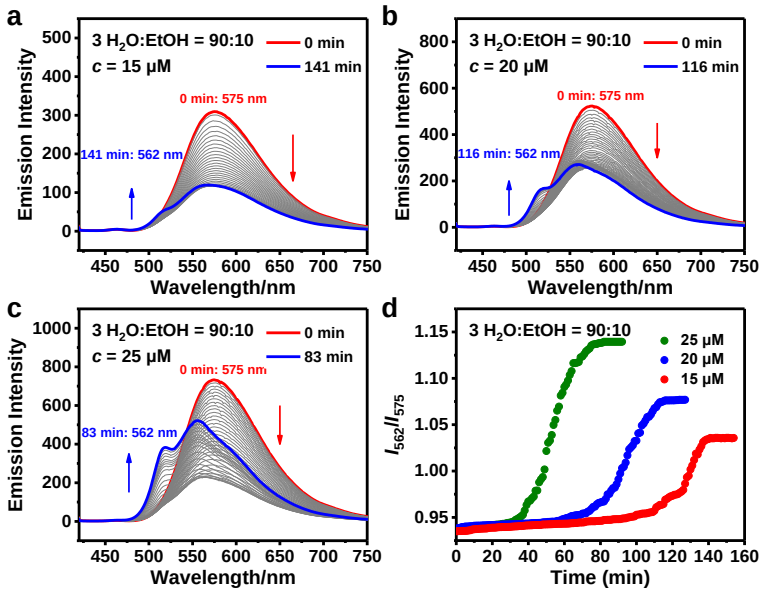

Figure S14. Time-dependent emission spectra of **3** in H_2O/EtOH (90:10, v:v) at different concentrations: 15 μM (a), 20 μM (b), 25 μM (c), respectively, 298 K. (d) Time-dependent relative emission intensity ratios of **3** (emission intensity at 562 nm/575 nm, I_{562}/I_{575}) at different initial concentrations in H_2O/EtOH (90:10, v/v), 298 K. λ_{ex} = 400 nm.

Self-assembly mode

Table S4. Crystal data of complexes **1-3**.

Complexes	**1**	**2**	**3**
Formula	$C_{50}H_{40}O_4N_4F_6PIr$	$C_{44}H_{32}N_4F_6PIr$	$C_{44}H_{32}N_4F_6PIr$
Formula weight	1098.23	953.93	953.93
Crystal system	Triclinic	Monoclinic	Triclinic
Temperature	200 K	200 K	200 K
Space Group	P-1	$P2_1/c$	P-1
Cell Lengths (Å)	a = 8.5229(9) b = 15.1560(16) c = 20.5241(19)	a = 22.1348(12) b = 11.7006(5) c = 15.5194(9)	a = 13.4045(6) b = 13.8201(7) c = 22.0022(11)
Cell Angles (°)	α = 70.301(3) β = 88.507(3) γ = 78.356(3)	α = 90 β = 102.085(2) γ = 90	α = 101.886(2) β = 106.065(2) γ = 98.232(2)
Cell Volume ($Å^3$)	2442.1(4)	3930.3(4)	3744.9(3)
Z	2	4	4
Density (g/cm^3)	1.542	1.681	1.692
F(000)	1132.0	1968.0	1880.0
h, k, lmax	10, 18, 24	28, 14, 19	17, 17, 28
Tmin, Tmax	0.606, 0.732	0.537, 0.704	0.330, 0.598
Absorption Coefficient/mm^{-1}	2.841	3.508	3.677
R(int)	0.1176	0.0906	0.0576
Data/restraints/ parameters	8755/0/615	8553/0/533	17114/0/1009
Goodness-of-fit on F^2	1.066	1.066	1.025
R_1[a] [$I > 2\sigma(I)$]	0.0477	0.0380	0.0273
wR_2[b] [$I > 2\sigma(I)$]	0.1156	0.0940	0.0659
R_1[a] (*all data*)	0.0592	0.0455	0.0365
wR_2[b] (*all data*)	0.1227	0.1003	0.0703
CCDC	2268065	2268064	2268063

[a] $R_1 = \sum || F_0 | - | F_c || / \sum | F_0 |$

[b] $wR_2 = [\sum w(F_0^2 - F_c^2)^2 / \sum w(F_0^2)^2]^{1/2}$

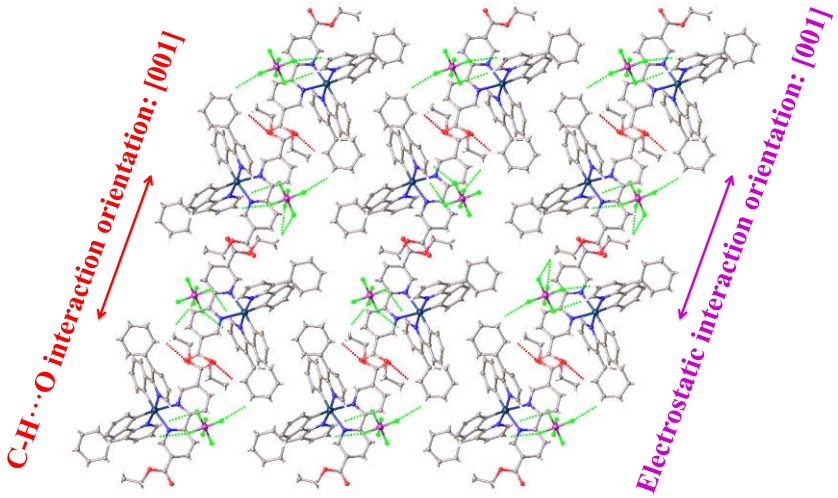

Figure S15. Self-assembly mode of **1** along the [100] direction.

Table S5. The distance and angle between the C-H ··O hydrogen bonds in crystal of **1**.

Type	Distance/Å	Angle/ °
C-H ··O	2.822	127.762

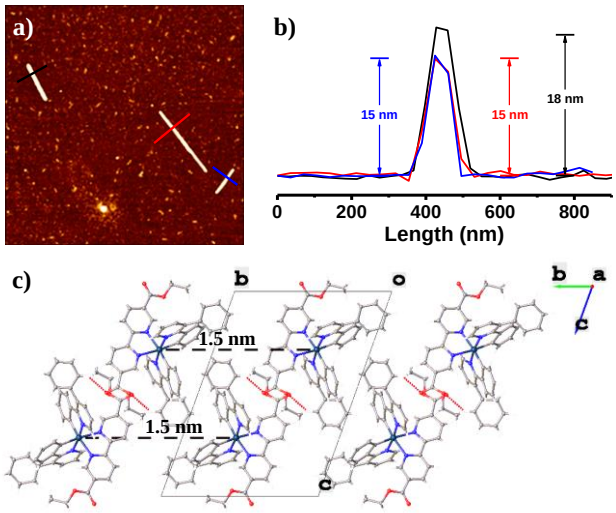

Figure S16. (a) AFM image of **1NF$_{seed}$**, (b) height profile of **1NF$_{seed}$** measured across the red, blue and black lines, (c) self-assembly mode of **1** in the crystal state along the [100] direction.

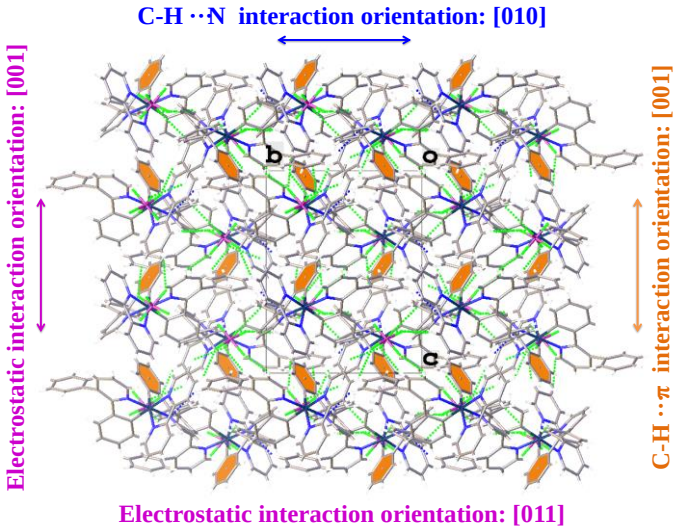

Figure S17. Self-assembly mode of **2** along the [100] direction. The orange planes represent the π planes of rotatable phenyl of C-H···π hydrogen bonding**.**

Table S6. The distances and angles between the C-H···π and C-H ··N hydrogen bonds in crystal of **2**.

Type	Distances/Å	Angles/ °
C-H ··π	3.163	81.910
C-H ··N	2.728	142.858

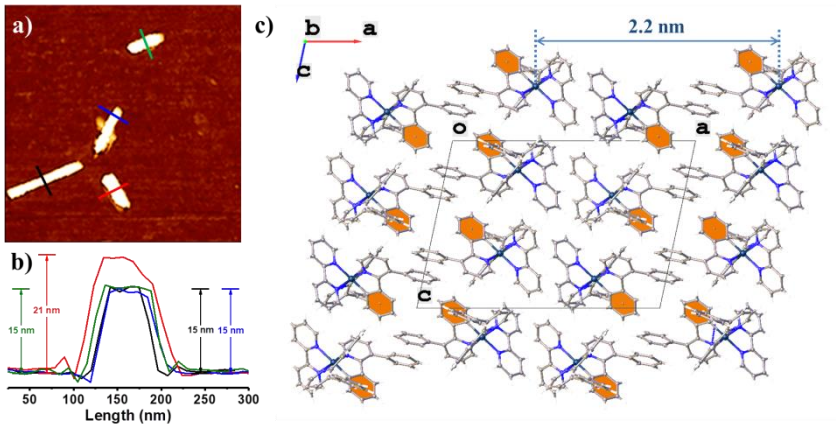

Figure S18. (a) AFM image of **2NS$_{seed}$**, (b) height profile of **2NS$_{seed}$** measured across the red, blue, green and black lines, (c) self-assembly mode of **2** in the crystal state along the [010] direction.

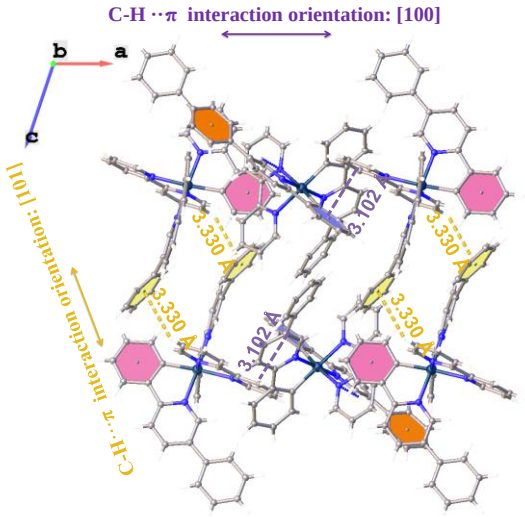

Figure S19. The C-H···π hydrogen bonding in the crystal of **3**. The PF_6^- counter-anion of each molecule is omitted for clarity.

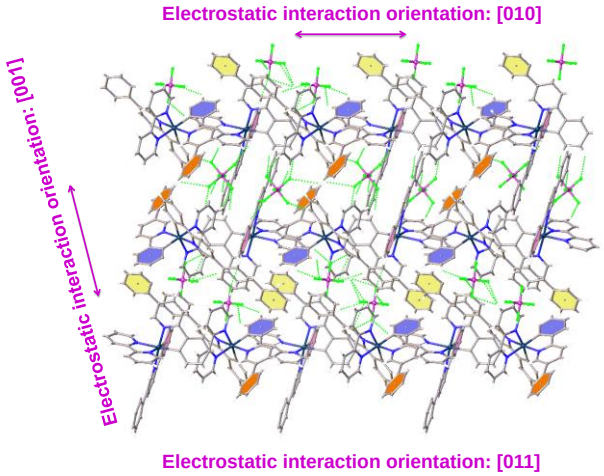

Figure S20. Self-assembly mode of **3** along the [100] direction. The pink and purple planes represent the π planes of 2-phenylpyridine of C-H···π hydrogen bonding. The orange and yellow planes represent the π planes of rotatable phenyl of C-H···π hydrogen bonding.

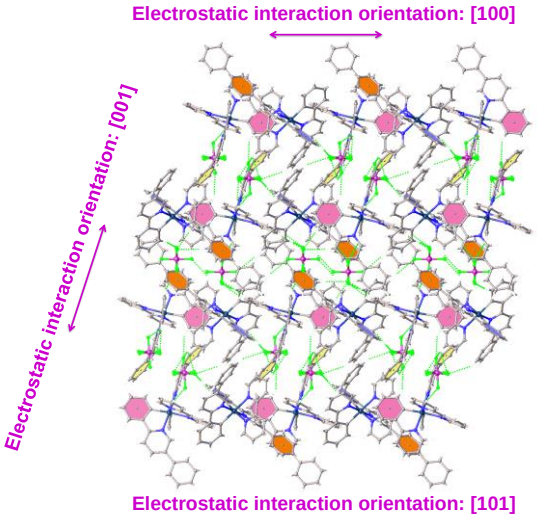

Figure S21. Self-assembly mode of **3** along the [010] direction. The pink and purple planes represent the π planes of 2-phenylpyridine of C-H···π hydrogen bonding. The orange and yellow planes represent the π planes of rotatable phenyl of C-H···π hydrogen bonding.

Table S7. The distances and angles between the C-H···π hydrogen bonds in crystal of **3**.

Type	Distances/Å	Angles/ °
C-H ··π	3.449	74.41
	3.107	72.65
	3.102	78.84
	3.330	71.75

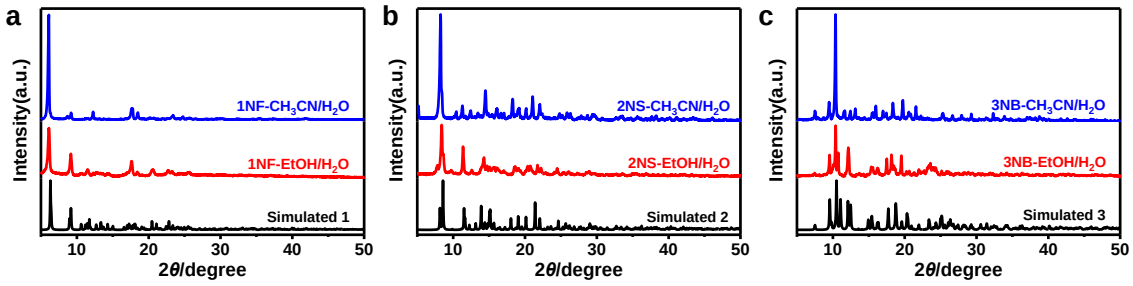

Figure S22. PXRD diffraction patterns of **1** (a), **2** (b) and **3** (c). **1NF**, **2NS** and **3NB** are obtained by centrifugation with water contents of 75%, 85% and 90%, respectively.

Seeded self-assembly

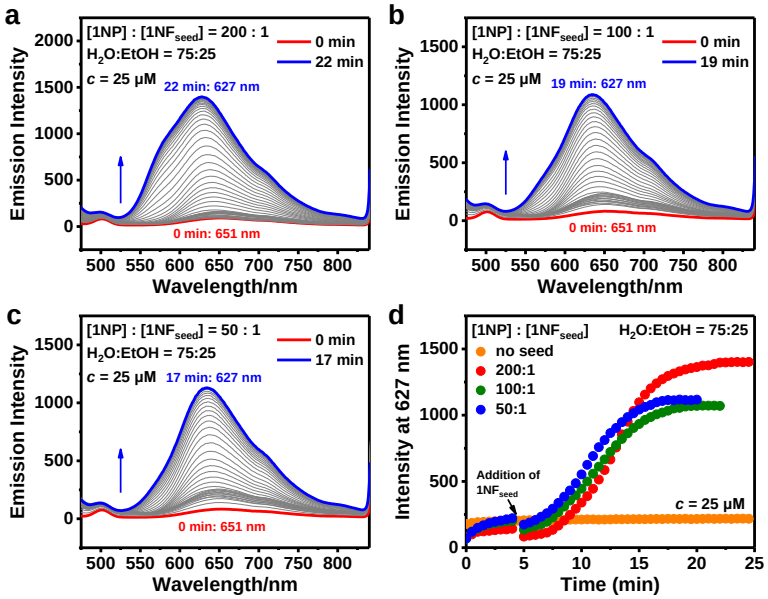

Figure S23. Time-dependent emission spectra observed upon mixing **1NP** and **1NF$_{seed}$** under [**1NP**]:[**1NF$_{seed}$**] = 200:1 (**a**), 100:1 (**b**), 50:1 (**c**) in H_2O/EtOH (75:25, v/v) at 25 μM. (d) Corresponding time courses of **1NP** initiated by the addition of **1NF$_{seed}$** under different conditions of [**1NP**]:[**1NF$_{seed}$**] in H_2O/EtOH (75:25, v/v) at 25 μM, 298 K. λ_{ex} = 430 nm.

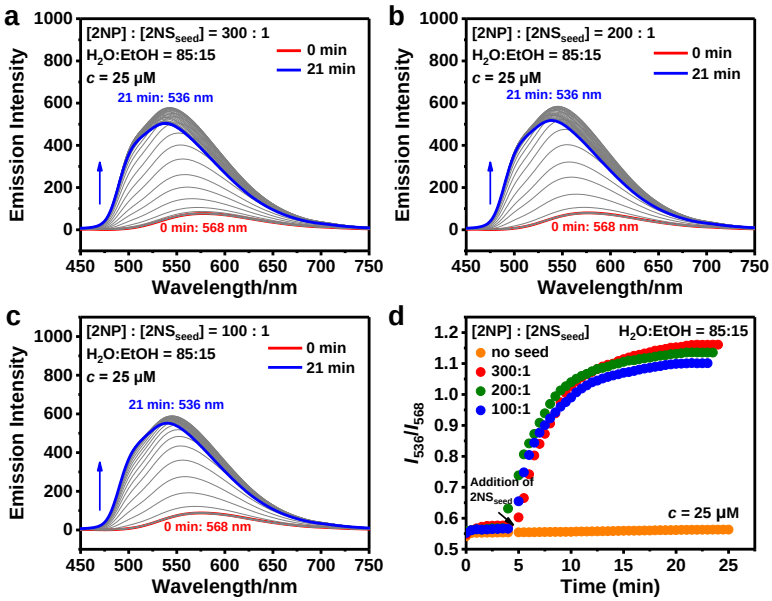

Figure S24. Time-dependent emission spectra observed upon mixing **2NP** and **2NS$_{seed}$** under [**2NP**]:[**2NS$_{seed}$**] = 300:1 (a), 200:1 (b), 100:1 (c) in H_2O/EtOH (85:15, v/v) at 25 μM. (d) Corresponding time courses of **2NP** initiated by the addition of **2NS$_{seed}$** under different conditions of [**2NP**]:[**2NS$_{seed}$**] in H_2O/EtOH (85:15, v/v) at 25 μM, 298 K. λ_{ex} = 400 nm.

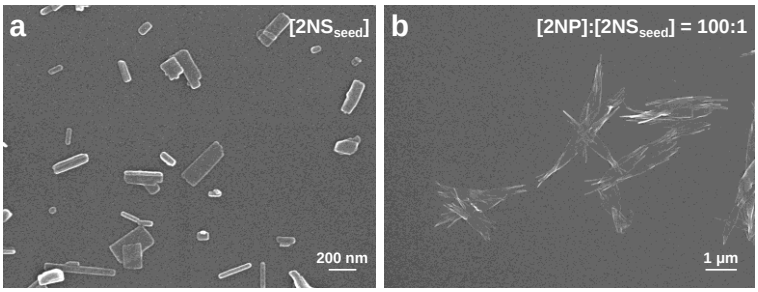

Figure S25. SEM images of **2NS$_{seed}$** (a) and **2NS** (b) obtained after the seeded self-assembly in H_2O/EtOH (85:15, v/v, 25 μM) under [**2NP**]:[**2NS$_{seed}$**] = 100:1 at 298 K.

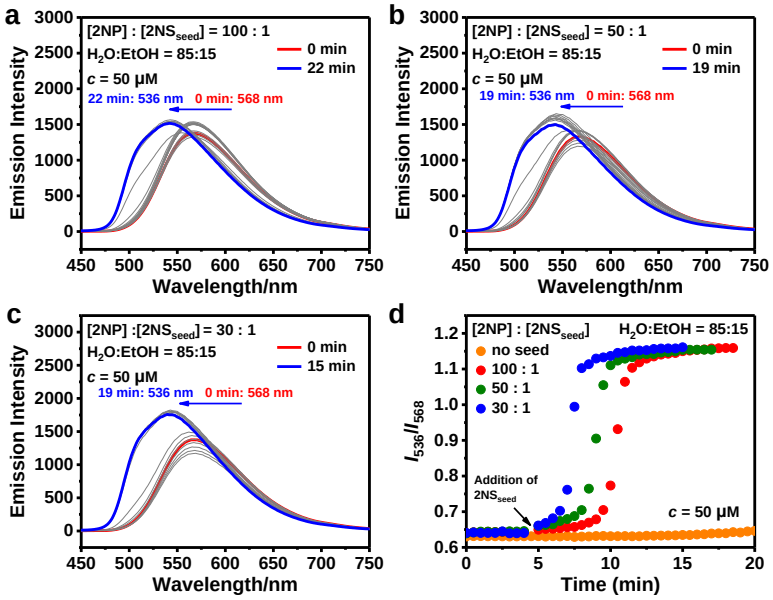

Figure S26. Time-dependent emission spectra observed upon mixing **2NP** and **2NS$_{seed}$** under [**2NP**]:[**2NS$_{seed}$**] = 100:1 (a), 50:1 (b), 30:1 (c) in H_2O/EtOH (85:15, v/v) at 50 μM. (d) Corresponding time courses of **2NP** initiated by the addition of **2NS$_{seed}$** under different conditions of [**2NP**]:[**2NS$_{seed}$**] in H_2O/EtOH (85:15, v/v) at 50 μM, 298 K. λ_{ex} = 400 nm.

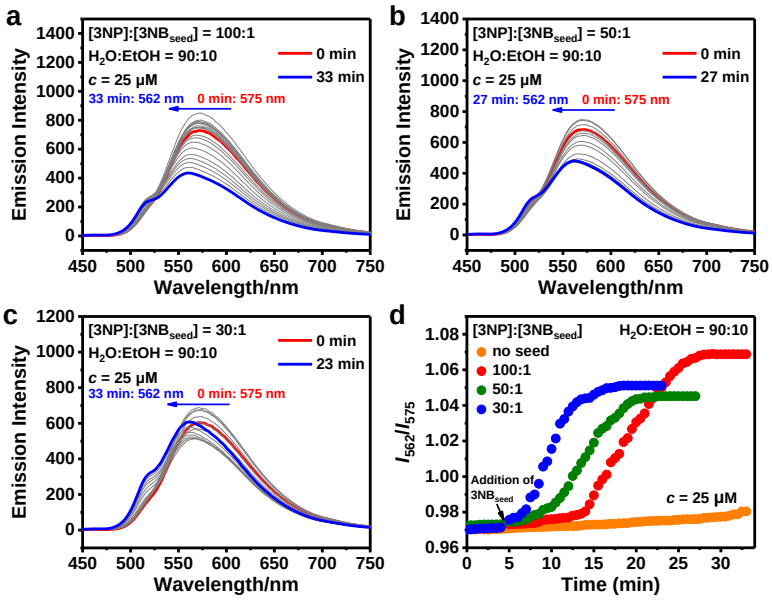

Figure S27. Time-dependent emission spectra observed upon mixing **3NP** and **3NB$_{seed}$** under [**3NP**]:[**3NB$_{seed}$**] = 100:1 (a), 50:1 (b), 30:1 (c) in H_2O/EtOH (90:10, v/v) at 25 μM. (d) Corresponding time courses of **3NP** initiated by the addition of **3NB$_{seed}$** under different conditions of [**3NP**]:[**3NB$_{seed}$**] in H_2O/EtOH (90:10, v/v) at 25 μM, 298 K. λ_{ex} = 400 nm.

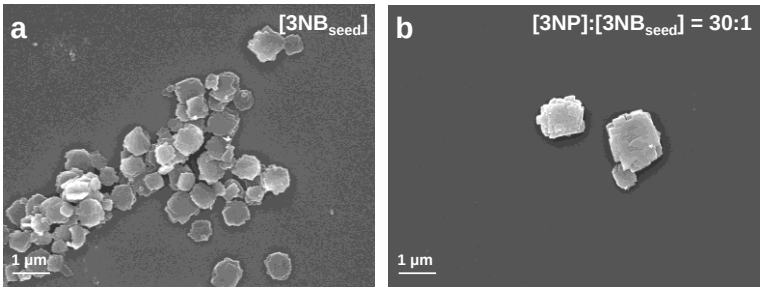

Figure S28. SEM images of **3NB$_{seed}$** (a) and **3NB** (b) obtained after the seeded self-assembly in H_2O/EtOH (90:10, v/v, 25 μM) under [**3NP**]:[**3NB$_{seed}$**] = 30:1 at 298 K.

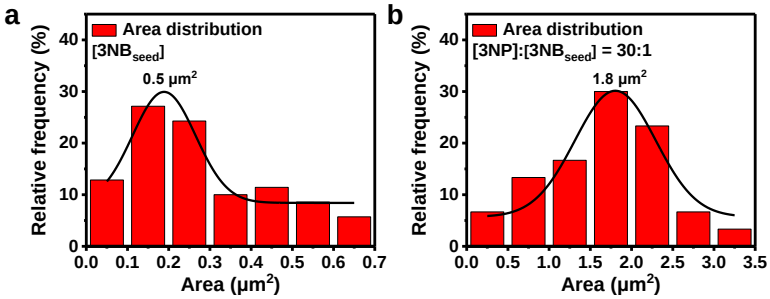

Figure S29. The area distribution of **3NB$_{seed}$** (a) and **3NB** (b) obtained after the seeded self-assembly in H_2O/EtOH (90:10, v/v, 25 μM) under [**3NP**]:[**3NB$_{seed}$**] = 30:1 at 298 K.

The multistep seeded self-assembly

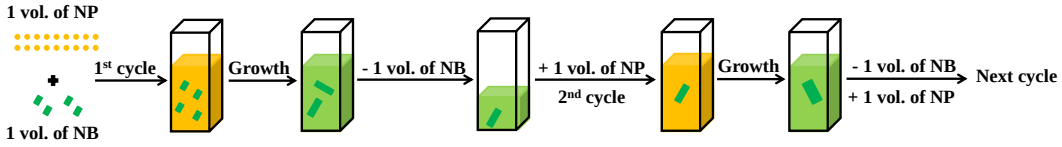

Figure S30. Schematic diagram of experimental operation process of the multistep seeded self-assembly.

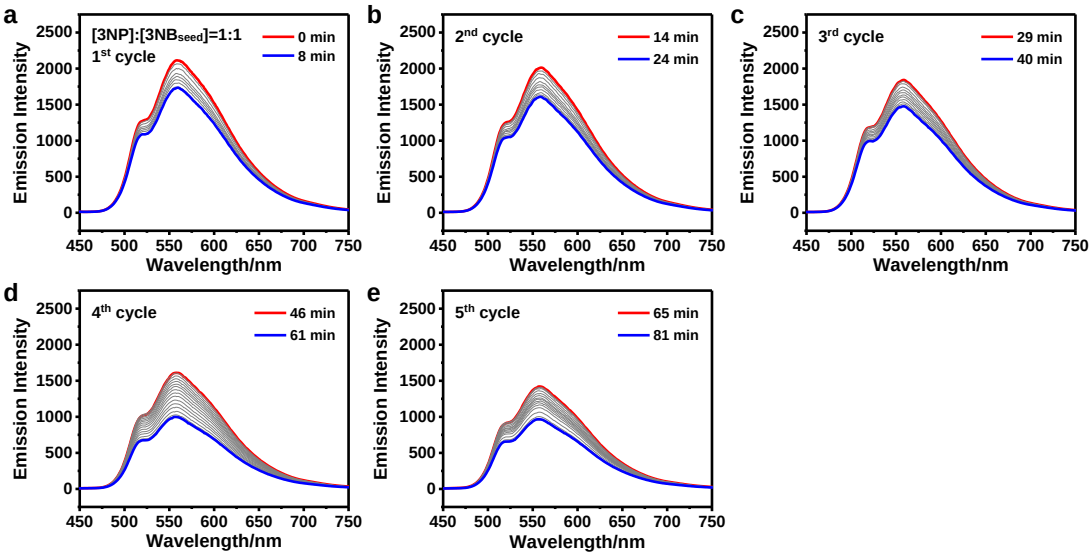

Figure S31. (a)-(e) Time-dependent emission spectra of the multistep seeded self-assembly. The initial vol. ratio of [**3NP**]:[**3NB$_{seed}$**] = 1:1 in H_2O/EtOH (90:10, v/v, 25 μM) at 298 K. λ_{ex} = 400 nm.

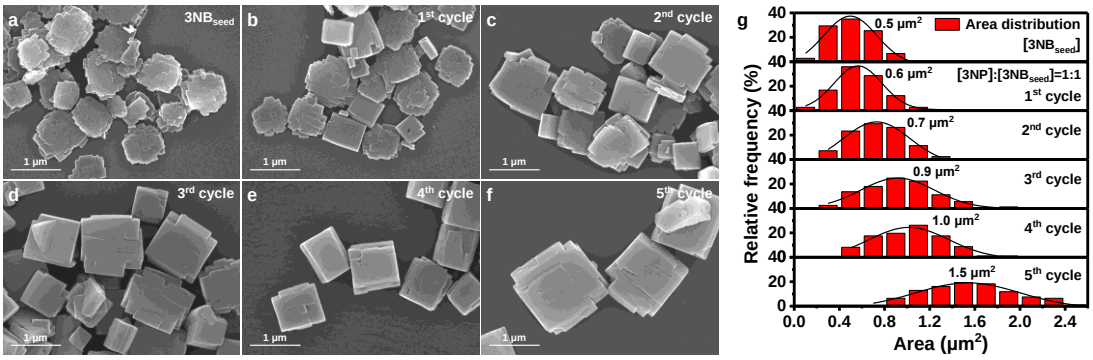

Figure S32. (a)-(f) SEM images of **3NB$_{seed}$** and **3NB** obtained after the multistep seeded self-assembly. (g) The area distribution of the corresponding **NB**.

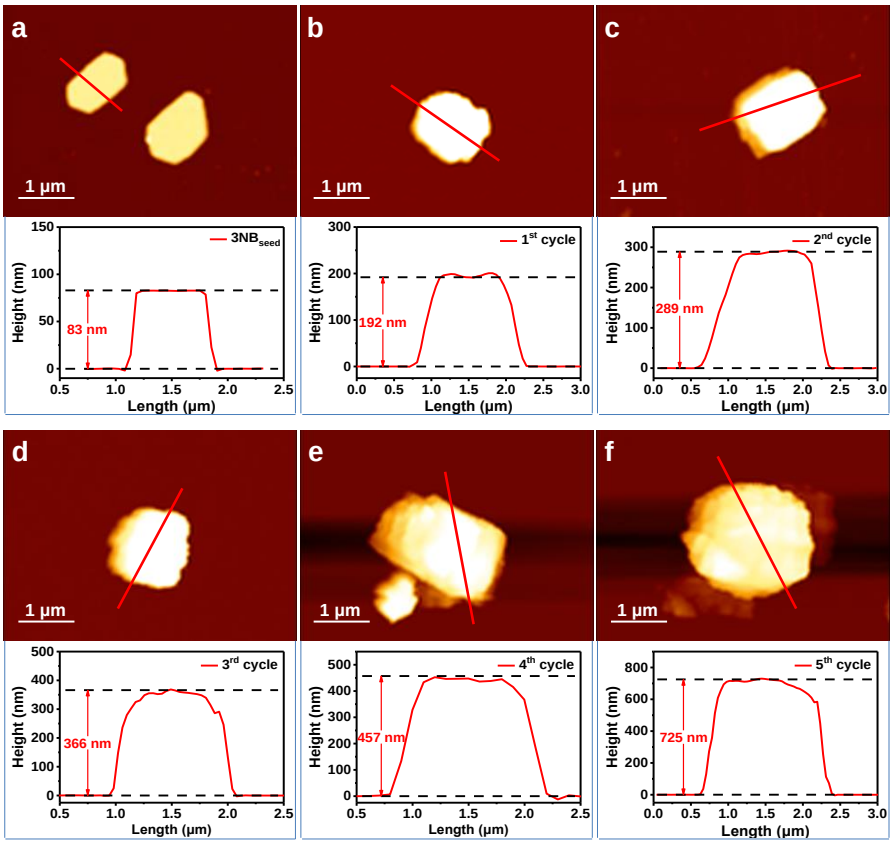

Figure S33. AFM images of **3NB$_{seed}$** and **3NB** obtained after the multistep seeded self-assembly in H_2O/EtOH (90:10, v/v, 25 μM) at 298 K. Height profile of **3NB$_{seed}$** and **3NB** measured across the red lines.

NMR spectra and HRMS of 1-3

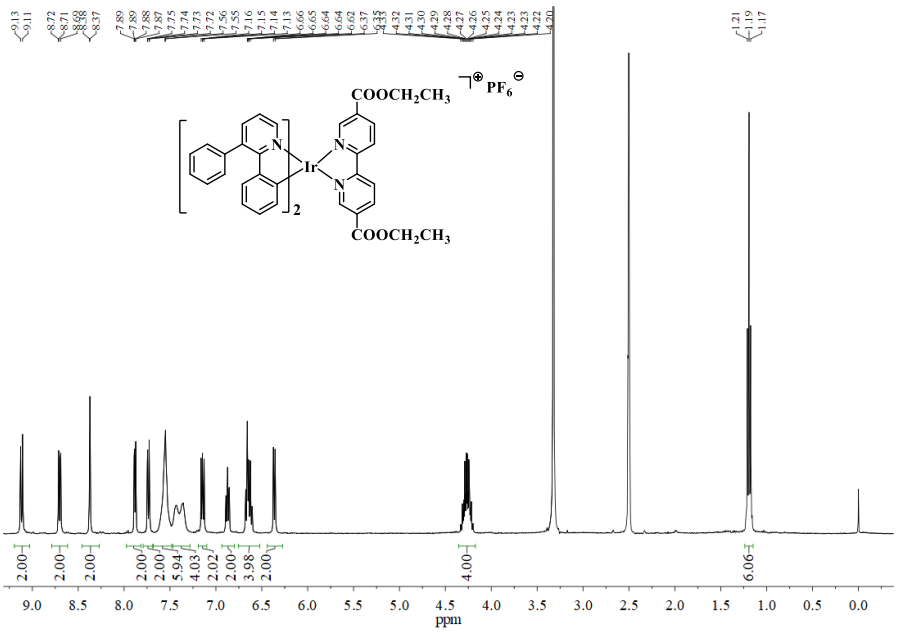

Figure S34. ^{1}H NMR spectrum of **1** in DMSO-d_6.

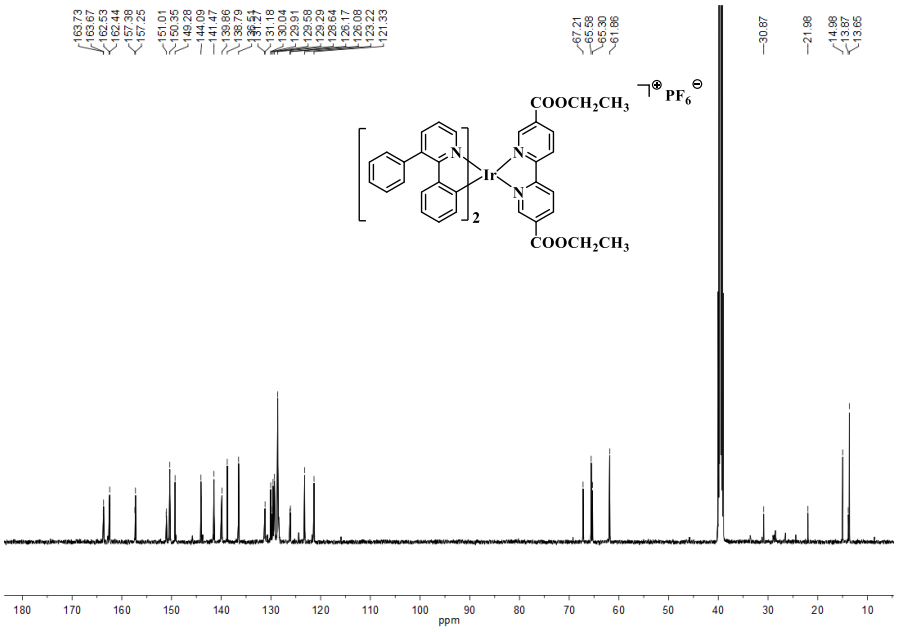

Figure S35. ^{13}C NMR spectrum of **1** in DMSO-d_6.

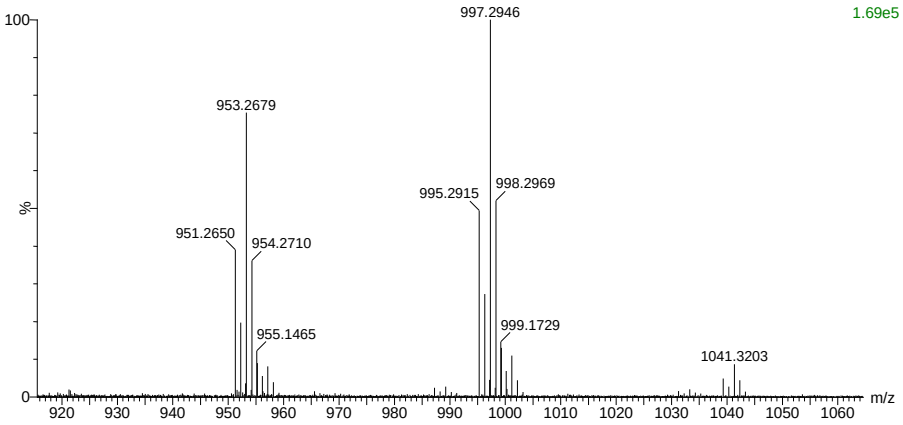

Figure S36. The HRMS of cationic portion of **1**.

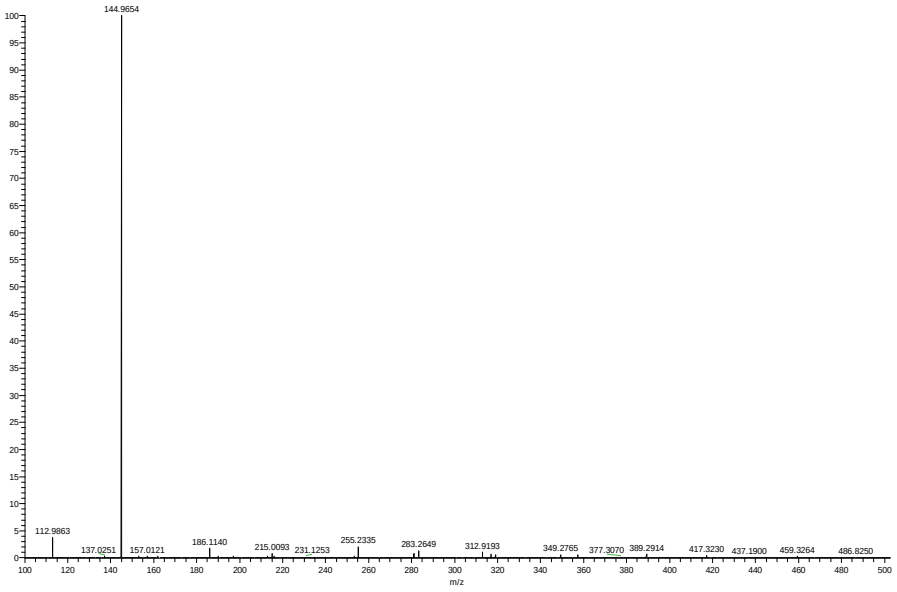

Figure S37. The HRMS of anionic portion of **1**.

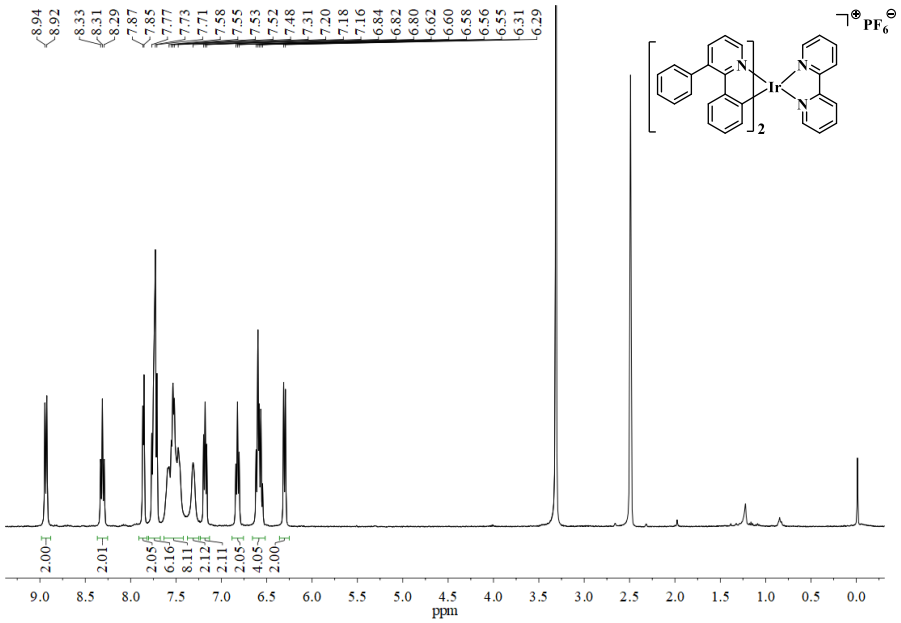

Figure S38. ^{1}H NMR spectrum of **2** in DMSO-d_6.

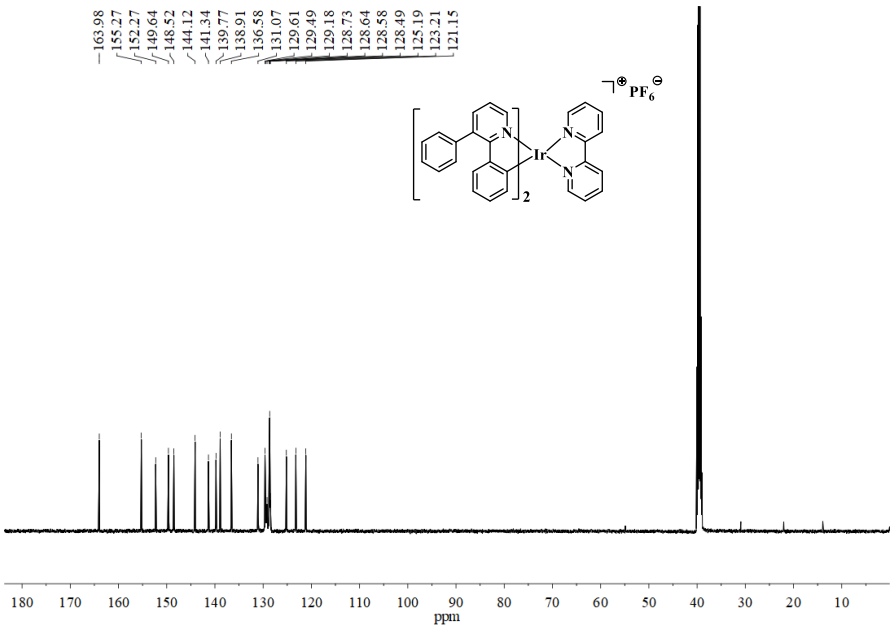

Figure S39. ^{13}C NMR spectrum of **2** in DMSO-d_6.

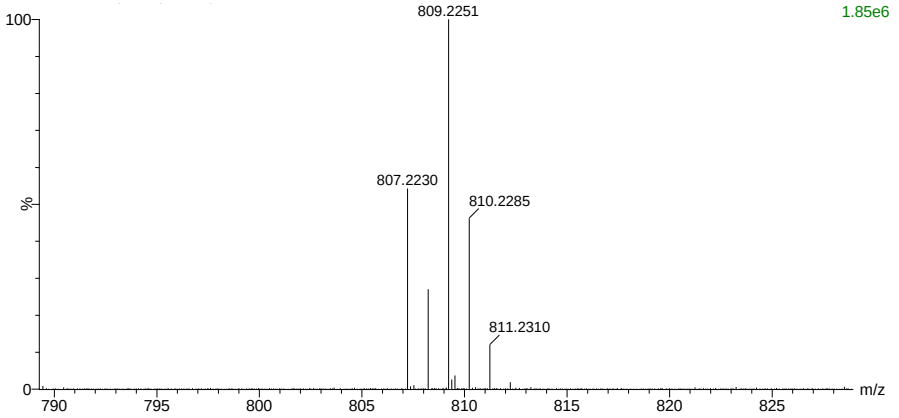

Figure S40. The HRMS of cationic portion of **2**.

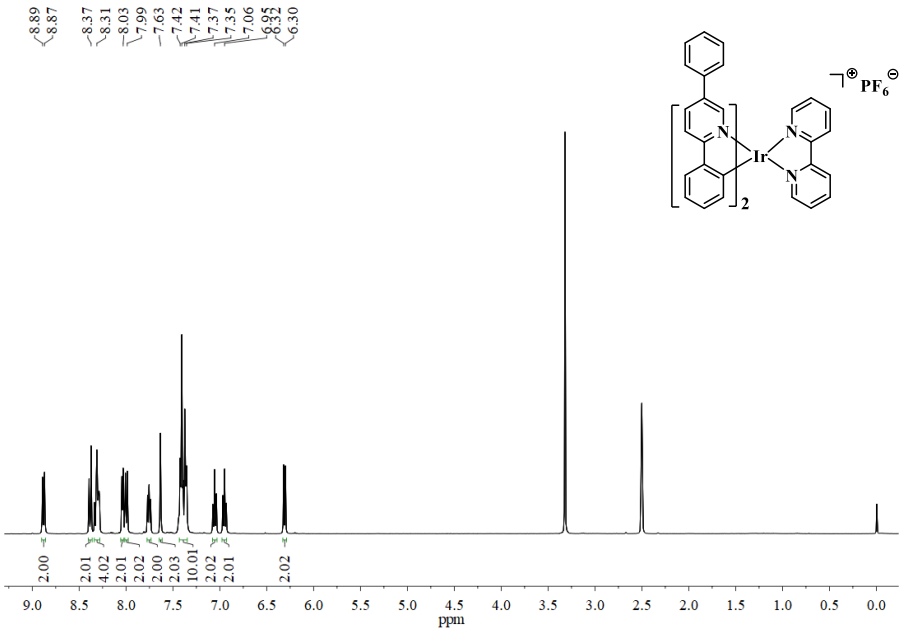

Figure S41. ^{1}H NMR spectrum of **3** in DMSO-d_6.

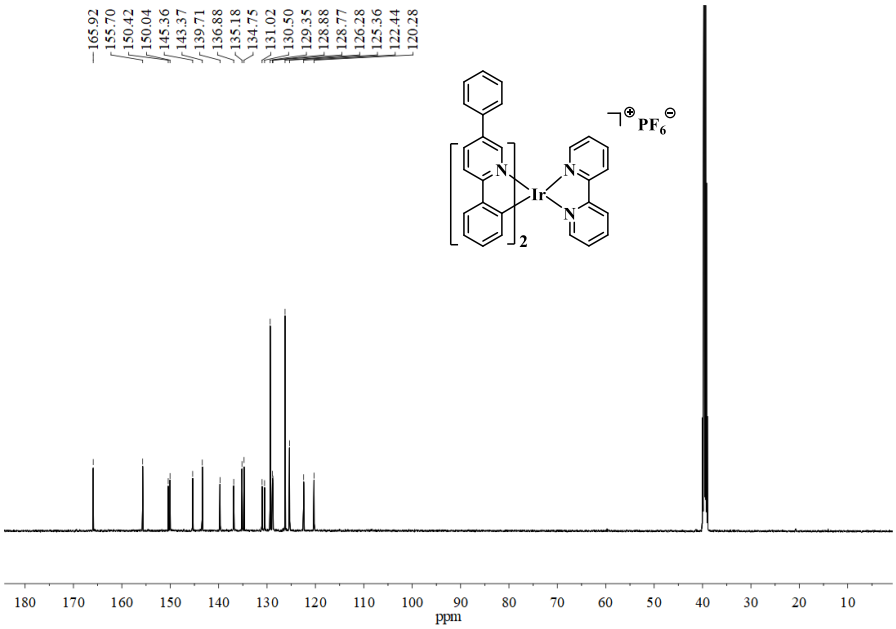

Figure S42. ^{13}C NMR spectrum of **3** in DMSO-d_6.

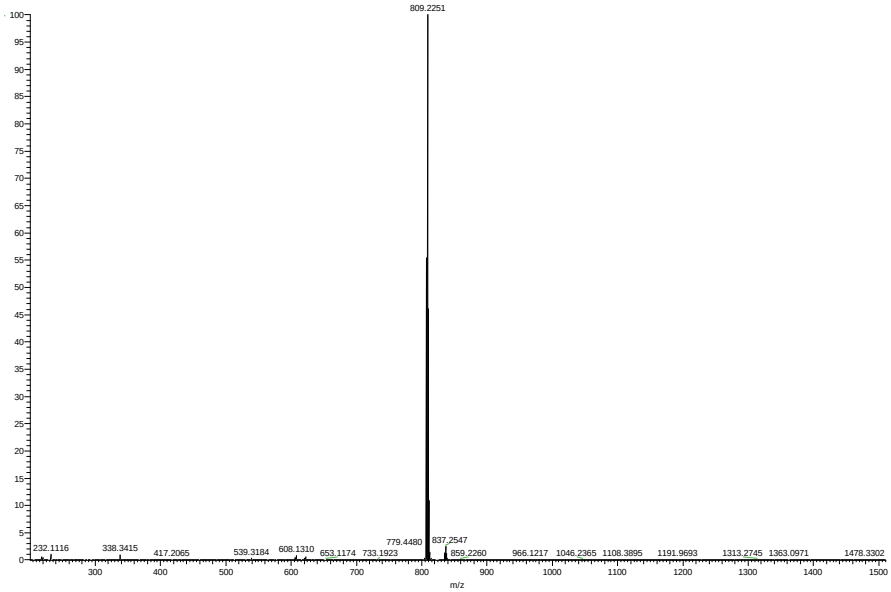

Figure S43. The HRMS of cationic portion of **3**.

References

1. SMART, Data collection software v. version 5.629 (Bruker AXS Inc., Madison WI., 2003).

2. SAINT, Data reduction software v. version 6.45 (Bruker AXS Inc., Madison WI., 2003).

3. G. M. Sheldrick, Crystal structure refinement with SHELXL. *Acta Crystallogr. C Struct. Chem.*, 2015, **71**, 3-8.

4. O. V. Dolomanov, L. J. Bourhis, R. J. Gildea, J. A. K. Howard and H. Puschmann, OLEX2: a complete structure solution, refinement and analysis program. *J. Appl. Crystallogr.*, 2009, **42**, 339-341.

5. A. J. Markvoort, H. M. M. ten Eikelder, P. A. J. Hilbers, T. F. A. de Greef and E. W. Meijer, Theoretical models of nonlinear effects in two-component cooperative supramolecular copolymerizations, *Nat. Commun.*, 2011, **2**, 509.

6. H. M. M. ten Eikelder, A. J. Markvoort, T. F. A. de Greef and P. A. J. Hilbers, An equilibrium model for chiral amplification in supramolecular polymers, *J. Phys. Chem. B*, 2012, **116**, 5291-5301.